



Southern Ocean control on atmospheric CO₂ changes across late-Pliocene Marine Isotope Stage M2

Suning Hou¹, Leonie Toebrock¹, Mart van der Linden¹, Fleur Rothstegge¹, Martin Ziegler¹, Lucas J. Lourens¹, Peter K. Bijl¹

¹ Department of Earth Sciences, Utrecht University, Utrecht, 3584 CB, the Netherlands

Correspondence to: Suning Hou (s.hou@uu.nl)

Abstract. During the Pliocene, atmospheric CO₂ concentrations ($p\text{CO}_2$) were similar to today's and global average temperature was ~ 3 °C higher. However, the relationships and phasing between variability in climate and $p\text{CO}_2$ on orbital time scales are not well understood. Specifically, questions remain about the nature of a lag of $p\text{CO}_2$ relative to benthic foraminiferal $\delta^{18}\text{O}$ in the late-Pliocene Marine Isotope Stage M2 (3300 kiloannum ago, ka), which was longer than during the Pleistocene. Here, we present a multi-proxy paleoceanographic reconstruction of the late-Pliocene subantarctic zone, which is today one of the major ocean sinks of atmospheric CO₂. New dinoflagellate cyst assemblage data is combined with previously published sea surface temperature reconstructions, to reveal past surface conditions, including latitudinal migrations of the subtropical front (STF) over the late-Pliocene at ODP Site 1168, offshore west Tasmania. We observe strong oceanographic variability at the STF over glacial-interglacial timescales, especially across the M2 (3320–3260 ka). By providing tight and independent age constraints from benthic foraminiferal $\delta^{18}\text{O}$, we find that, much more than benthic $\delta^{18}\text{O}$ or local SST, latitudinal migrations of the STF are tightly coupled to $p\text{CO}_2$ variations across the M2. Specifically, a northerly position of the STF during M2 deglaciation coincides with generally low $p\text{CO}_2$. We postulate that the efficiency of the Southern Ocean carbon outgassing varied strongly with migrations of the STF, and that is in part accounted for the variability in $p\text{CO}_2$ across M2.

1 Introduction

As the largest exogenic carbon reservoir on Earth, the ocean plays a pivotal role in regulating Earth's climate, through the balance between CO₂ uptake and outgassing (Sabine et al., 2004; Friedlingstein et al., 2022). Upwelling in the polar frontal zone flushes respired CO₂ from deep ocean into the atmosphere (Process 1 in Fig. 1a). This process is predominantly controlled by shifts in sea ice extent and westerlies over glacial and interglacial climates, which move the latitudinal position of oceanic fronts in the Southern Ocean (Toggweiler et al., 2006; Skinner et al., 2010; Rae et al., 2018). Moreover, the biological carbon pump absorbs dissolved CO₂ and removes it from surface waters via export productivity (Martin, 1990; Martínez-García et al., 2014; Thöle et al., 2019), thereby reducing surface dissolved inorganic carbon (DIC) which enhances CO₂ diffusion from the atmosphere (Process 2, 3 in Fig. 1a; Egleston et al., 2010; Gruber et al., 2023). This process mainly takes place at the boundary between the subantarctic and subtropical zone (SAZ), where ocean surface temperature (which has a negative



30 influence on CO₂ uptake), ocean stratification (negative), salinity (negative) and DIC (negative) determine CO₂ diffusion
efficiency. The past decades have seen profound changes in sea surface temperature (SST), salinity (SSS) and the stratification
of the SAZ surface waters (Sabine et al., 2004). How these processes will affect the ability of the ocean to act as climate change
mitigator in the coming decades, and the amount of excess CO₂ that would consequently remain in the atmosphere is currently
uncertain (Gruber et al., 2023). This creates a critical uncertainty in the projections of atmospheric CO₂ concentration (*p*CO₂)
35 and the resulting effects on climate and sea level, given emission pathway scenarios (IPCC, 2019; Burton et al., 2023).

Reconstructing Southern Ocean conditions in past deglaciation phases might help in understanding interactions between
atmospheric climate and ocean conditions. The late-Pliocene is marked by dominant obliquity-controlled benthic foraminiferal
oxygen isotope ($\delta^{18}\text{O}_{\text{bf}}$) increases that have been interpreted as glaciation/cooling phases (e.g., Tiedemann et al., 1994;
40 Shackleton et al., 1995; Lisiecki and Raymo, 2005). The most prominent of which is the Marine Isotope Stage (MIS) M2
(3312–3264 ka; Keigwin, 1987), the deglaciation of which terminates into the mid-Piacenzian Warm Period (mPWP, 3264–
3025 ka). Questions remain on its forcing, but also whether this event is mostly reflective of deep-ocean cooling or ice volume
increase. Antarctic ice-proximal lithological and biomarker records suggest surface cooling and ice advance and therefore ice
volume increase is involved (McKay et al., 2012; Cook et al., 2013; Patterson et al., 2014), perhaps also on the northern
45 hemisphere as suggested by ice-rafted detritus (Flesche Kleiven et al., 2002). In contrast, bottom water temperature (BWT;
Braaten et al., 2023) and ice sheet (Yamane et al., 2015; Mas e Braga et al., 2023) studies suggest limited ice volume change
across M2–mPWP transition.

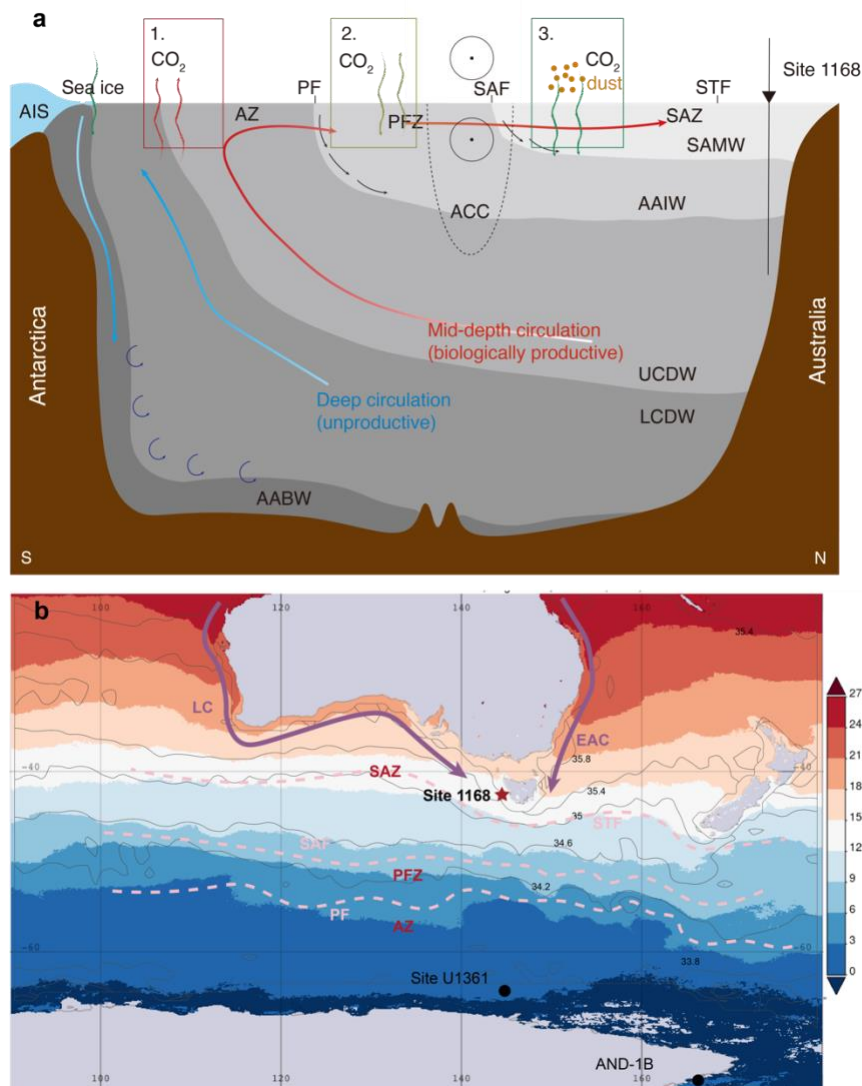
The subsequent mPWP is the most recent time whereby climate conditions were at times equilibrated to modern-like *p*CO₂ of
50 about 400 parts per million (De la Vega et al., 2020; CENCO2PIP CONSORTIUM, 2023). Specifically, MIS KM5c (3205
ka) has been a focus point of study because of the similar orbital configuration as today (Haywood et al., 2020). The Pliocene
Model Intercomparison Project Phase 2 (PLIOMIP 2; Haywood et al., 2020) compares an ensemble of numerical models run
under similar boundary conditions, to global compilations of proxy data from sediment cores (e.g., of sea surface temperature,
SST; McClymont et al., 2020). From these efforts, accurate global average temperature, climate sensitivity to *p*CO₂ (2.6–4.8
55 °C; Haywood et al., 2020) and increased hydrological cycle (wetter equatorial regions, drier subtropical regions; Han et al.,
2021) were reconstructed.

The nature and forcing factors behind the M2–mPWP glacial-interglacial transition (3320–3260 ka) is not well understood.
High-resolution *p*CO₂ reconstructions for the late-Pliocene reveal low amplitude variability on orbital time scales (De la Vega
60 et al., 2020), i.e., of similar magnitude as that in the late Pleistocene, but the trends in *p*CO₂ and $\delta^{18}\text{O}_{\text{bf}}$ are not as synchronous
as in the Pleistocene. Specifically, while PLIOMIP2 demonstrates that overall high *p*CO₂ in the late-Pliocene is likely
responsible for the warmer-than-modern climates (Burton et al., 2023), questions remain on the exact phase relationship
between *p*CO₂ change and $\delta^{18}\text{O}_{\text{bf}}$ across the M2–mPWP transition. Available records seem to suggest that *p*CO₂ lags changes



65 in $\delta^{18}\text{O}_{\text{bf}}$ and (sub)surface cooling about 10–20 kyr (De La Vega et al., 2020; van der Weijst et al., 2022), or in any case are on these time scales not directly related through climate sensitivity to radiative forcing. We further note that collective knowledge on high-resolution $p\text{CO}_2$ change across the M2/mPWP interval is restricted to one record. Mg/Ca- and clumped isotope-based deep-sea cooling also demonstrate a lag relative to $\delta^{18}\text{O}_{\text{bf}}$ (Braaten et al., 2023). These leave the question open how $p\text{CO}_2$, ocean and cryosphere influenced each other over the M2-mPWP transition.

70 Here we investigate how the surface oceanography of one of the major ocean carbon sinks, the SAZ, changed through the M2-mPWP transition, and infer the implications for the carbon uptake efficiency of the region. We present a multiproxy reconstruction of paleoceanographic conditions from Ocean Drilling Program (ODP) Site 1168 (Fig. 1b), offshore west Tasmania, which is located close to the modern position of the subtropical front (STF) and the centre of the modern subantarctic/subtropical zone. We reconstruct surface ocean conditions based on dinoflagellate cyst assemblages, a
75 microplankton group that is strongly tied to specific ocean surface conditions: SST, SSS and nutrients (Thöle et al., 2023). These strict affinities are applied together with previously published biomarker-based sea surface temperature for a detailed reconstruction of changing oceanographic conditions: the latitudinal position of the subtropical front through time, which potentially deciphers the delayed $p\text{CO}_2$ change with respect to $\delta^{18}\text{O}_{\text{bf}}$.



80 **Figure 1:** (a) Schematic view of the ocean circulation in the Southern Ocean between Antarctica and Australia. Arrows in the ocean
 denote southern overturning circulation (blue), mid-depth overturning circulation (red); SAMW=subantarctic mode water,
 AAIW=Antarctic Intermediate Water, U/LCDW=Upper/Lower Component Deep Water, AABW=Antarctic Bottom Water,
 ACC=Antarctic Circumpolar Current; Curvy arrows denote CO₂ uptake or outgassing processes (1. Deep ocean degassing, red; 2.
 85 Physical diffusion, spring green; 3. Biological carbon pump, green). (b) Modern site location of ODP Site 1168. Colors indicate sea
 surface temperatures; Contours indicates sea surface salinity; Grey blocks indicate modern coastline and sea ice extent. Purple
 arrows denote ocean currents (LC=Leeuwin Current, EAC=East Australia Current). Pink dashed lines denote oceanic fronts
 (STF=Subtropical Front, SAF=Subantarctic Front, PF=Polar Front) and zones in between (SAZ=Subtropical/Subantarctic Zone,
 PFZ=Polar Frontal Zone, AZ=Antarctic Zone) are mentioned in red. Data, map and visualization were generated using the Giovanni
 90 online data system (<https://giovanni.gsfc.nasa.gov/giovanni/>) developed and maintained by the National Aeronautics and Space
 Administration Goddard Earth Sciences Data and Information Services Center (Acker and Leptoukh, 2007). SST and SSS data are
 derived from MODIS-Aqua provided to Giovanni by the Ocean Biology Distributed Active Archive Center.



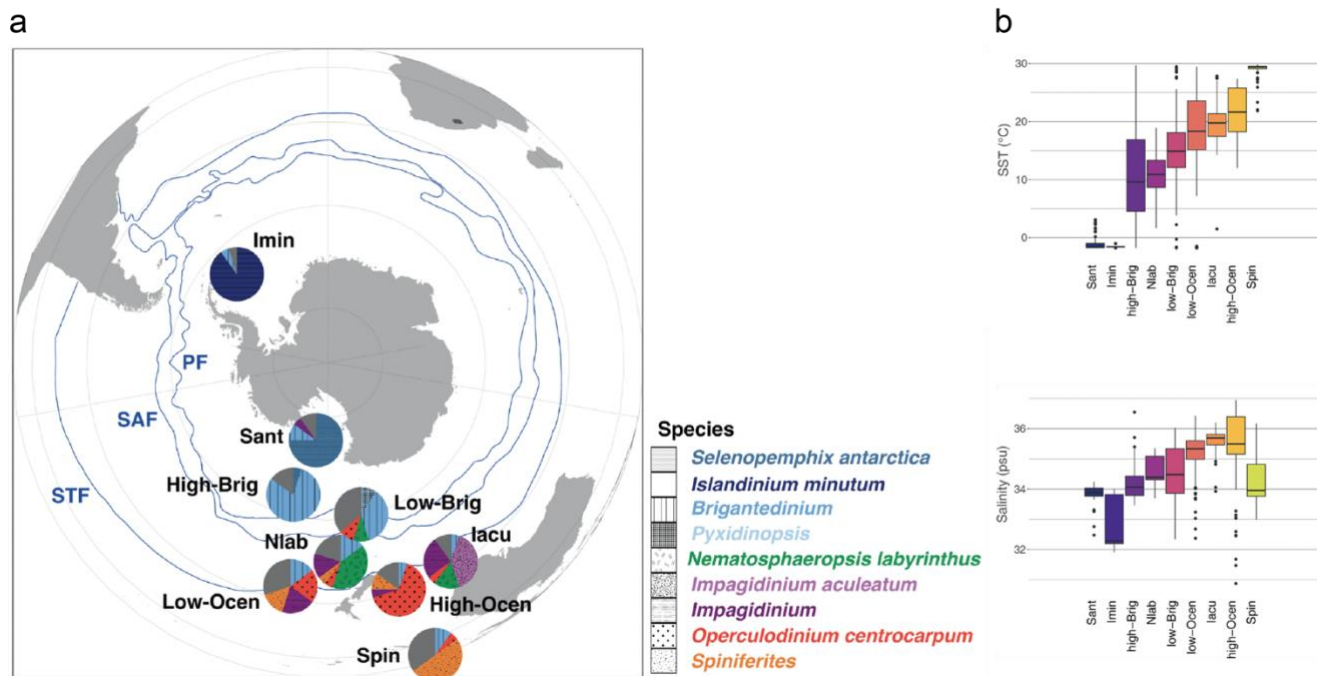
2 Materials and Methods

2.1 Study site

ODP Site 1168 (42°36.5809'S, 144°24.7620'E; 2463 meters modern water depth; Fig. 1a) was drilled on the continental slope
95 offshore west Tasmania (Exon et al., 2001). The Pliocene part of the sequence contains greenish-grey foraminifer-bearing
nannofossil ooze with significant detrital clay input (Exon et al., 2001). At present, the STF is located closely over this site,
which separates warm (>17 °C), saline subtropical waters from comparably cold (<13 °C) and fresh subantarctic water masses
(Heath, 1985; Exon et al., 2001). Site 1168 is characterized by a modern SST seasonality ranging from 13–17 °C (winter–
summer) and a modern BWT of 2.5 °C.

100 2.2 Palynology

We processed 56 samples for palynology in the late-Pliocene interval. Processing used standard procedures of the GeoLab of
Utrecht University (e.g., Brinkhuis et al., 2003). Briefly, this involves first spiking samples with *Lycopodium clavatum* spores
prior to palynological processing to allow for quantification of the absolute number of dinocysts per sample (Stockmarr, 1971).
Samples were then treated with 30% hydrochloric acid and ~38–40% hydrofluoric acid to concentrate the acid-resistant organic
105 residue. The isolation of the 10–250 µm fraction was established using nylon mesh sieves and an ultrasonic bath to break up
agglutinated particles of the residue. Palynomorphs were counted up to a minimum of 200 identified dinocysts if possible.
Taxonomy follows that stated on palsys.org (see Bijl and Brinkhuis, 2023; last access 8-1-2024). Functional ecological
dinocyst grouping follows those derived from modern assemblages (Fig. 2; Thöle et al., 2023). Notably, *Nematosphaeropsis*
labyrinthus is characteristic for the Nlab cluster that prevails south of the STF; *Impagidinium aculeatum*, *Operculodinium*
110 *centrocarpum* and *Spiniferites* spp. thrive in the Iacu-, high-Ocen-, and Spin- clusters to the north of the STF (Fig. 2). A STF
index is then defined as South of STF/(South+North of STF) in order to quantitatively demonstrate the migration of STF,
although the index does not directly indicate the latitudinal position of STF. A higher value of the index indicates that the STF
is positioned relatively further north, and vice versa. There are additional dinocysts assemblages specific for Southern Ocean
zones further away from the STF (Fig. 2; Thöle et al., 2023). This creates an opportunity to reconstruct in detail past changes
115 in the latitudinal position of the STF through the late-Pliocene, and with that, the oceanographic changes in the
subantarctic/subtropical carbon sink. In addition, given that *Impagidinium pallidum*, which is a typical bipolar cold-water
species in the modern ocean (the only *Impagidinium* in the ice-proximal Sant cluster, Fig. 2a), seems to have an ambiguous
paleo-affinity (De Schepper et al., 2011) and generally low abundance and widespread occurrence in the modern Southern
Ocean (Thöle et al., 2023), it is not separated from the other *Impagidinium* in the grouping. Moreover, because the latitudinal
120 position of the STF is representative of the oceanographic fronts associated with ACC and has implications for the sea ice
extent further south, our reconstructions also have implications for the ability of the polar frontal zone to emit CO₂ to the
atmosphere.



125 **Figure 2:** (a). Schematic representation of the generalized biogeographic distribution of dinocysts in Southern Ocean surface
 sediments. Pies represent average assemblage composition of the nine clusters described in this paper. Position of these pies represent
 their typical latitudinal band of occurrence. Also plotted are the frontal systems (blue lines, STF = Subtropical Front, SAF =
 Subantarctic Front, PF = Polar Front). The Subantarctic Zone (SAZ) is the water mass between the STF and PF. (b) Comparison
 of sea surface temperature and sea surface salinity in different clusters for the 9-cluster solution of the sh_655 data set. The median,
 130 25% – 75% quantiles and 95% confidence interval are indicated by the black line, boxes and whiskers, respectively. Modified from
 Thöle et al. (2023).

2.3 Benthic foraminiferal stable isotopes

Each sediment sample was freeze-dried, washed over a 63 µm sieve, oven-dried at 50 °C and then dry-sieved into different
 size fractions. We mainly picked tests of *Cibicidoides mundulus* from the 250–355 µm size fraction for our measurements.
 135 The picked specimens were cracked between two glass plates after which the test fragments were ultrasonicated in deionized
 water (3*30 s) to remove adhering sediment, organic lining and nannofossils. The test fragments were dried at room
 temperature overnight. In order to obtain enough material, other benthic species are also processed. We use *Cibicidoides*
mundulus and *Cibicidoides (Planulina) wuellerstorfi* for both stable carbon and oxygen.

140 Stable isotope measurements were performed using a Thermo Scientific MAT 253 Plus and a Thermo Scientific MAT 253
 mass spectrometer at the GeoLab of Utrecht University. Both mass spectrometers were coupled to Thermo Fisher Scientific



Kiel IV carbonate preparation devices. CO₂ gas was extracted from carbonate samples with phosphoric acid at a reaction temperature of 70°C. Since both instruments are equipped for clumped isotope analysis, a Porapak trap included in each Kiel
145 IV carbonate preparation system was kept at -40°C to remove organic contaminants from the sample gas. Between each run, the Porapak trap was heated at 120°C for at least 1 h for cleaning. Every measurement run included a similar number of samples and carbonate standards (Kocken et al., 2019). 3 carbonate standards (ETH-1, 2, 3). Two additional reference standards (IAEA-C2 and Merck) were measured in each run to monitor the long-term reproducibility and stability of the instrument. The δ¹³C and δ¹⁸O values (reported relative to the Vienna Pee Dee Belemnite (VPDB) scale) of IAEA-C2 showed an external
150 reproducibility (standard deviation) of 0.06 ‰ and 0.06 ‰, respectively.

2.4 Bulk carbonate stable isotopes

Bulk carbonate isotopes were measured as additional stratigraphic tool alongside the benthic δ¹³C and δ¹⁸O. For 118 samples, between 50–100 µg of powdered sediment was analysed on a Thermo Finnigan GasBench II system, coupled to a Thermo Delta-V mass spectrometer. Homogenized samples were transferred to sealable vials which were flushed with helium for 5
155 minutes per vial, to remove atmospheric oxygen and carbon. In each run, 65 samples were then treated with H₃PO₄ at a temperature of 72°C together with carbonate standards NAXOS (11 times) and IAEA-603 (4 times) for the purpose of calibration. All isotope values are reported against VPDB. Analytical precision, as determined by the SD of NAXOS was better than 0.08‰ for δ¹⁸O and 0.04‰ δ¹³C.

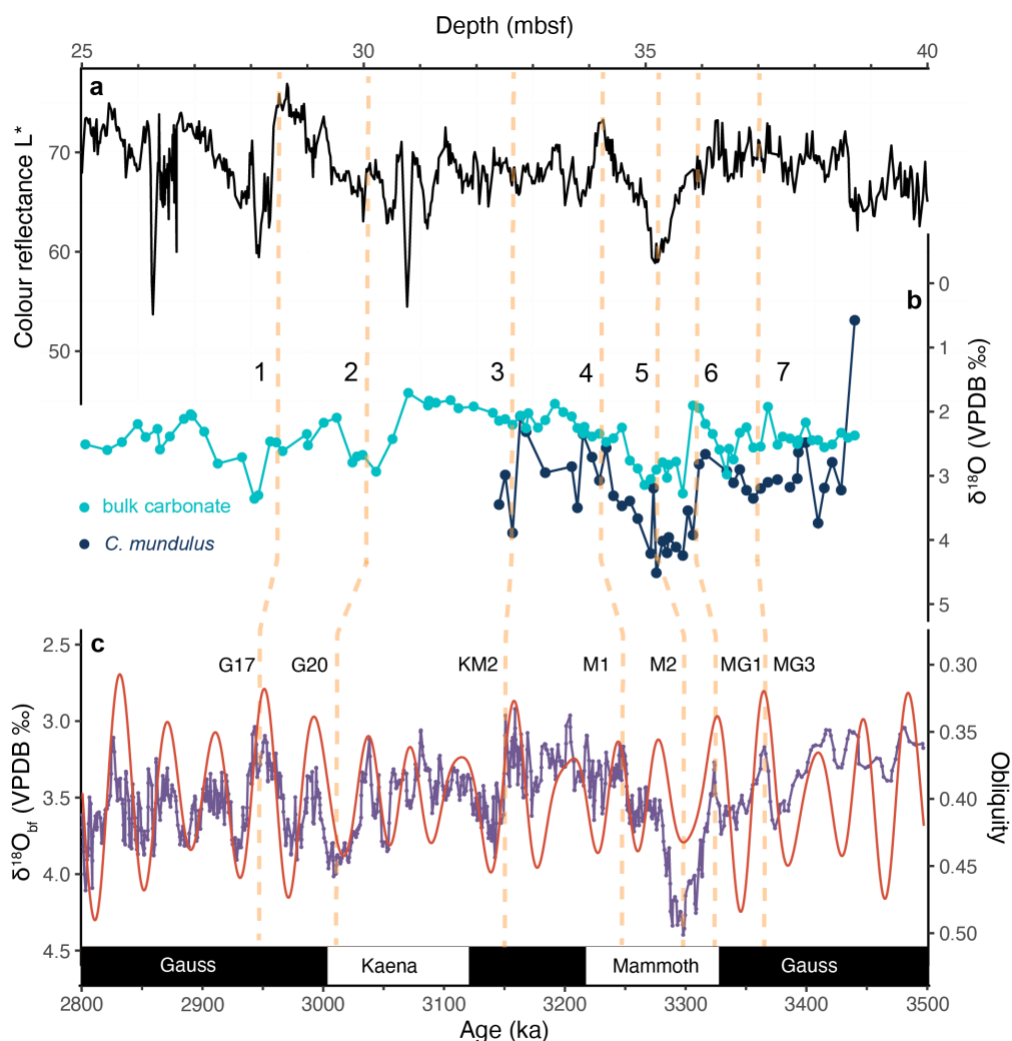
3 Results

160 3.1 Stable isotopes and age model

The post-expedition age model of sediments from ODP Site 1168 comprises of biostratigraphic constraints from nannofossils, foraminifera, diatoms and dinoflagellate cysts, paleomagnetic constraints, and for the Pleistocene identifications of marine isotope stages from benthic foraminiferal isotopes (Stickley et al., 2004). For the Pliocene-Pleistocene part of the record, the paleomagnetic constraints, which come from Hole B, are structurally offset by around 50m/1 million years from
165 biostratigraphic datums and Pleistocene marine isotope stages that come from Hole A, even at splice depth (see Stickley et al., 2004). For a high-resolution age model of the late-Pliocene section at Hole 1168A, we generated new benthic foraminiferal and bulk carbonate stable isotope data across the suspected late-Pliocene interval and compared these to the shipboard colour reflectance data (Exon et al., 2001). Cyclicity in both were then compared to orbital cycles seen in the CENOGRID (Westerhold et al., 2020) and LR04 benthic foraminifer oxygen isotope stack (Lisiecki and Raymo, 2005) (Fig. 3). Since all
170 our new data and the stratigraphic constraints except the paleomagnetic reversals derive from Hole A, we decided for the purpose of this study to ignore the offset paleomagnetic constraints from Hole B (as published in Stickley et al. (2004) and updated in Hou et al. (2023a)) for now, and recommend that later studies should first revisit the composite depth, stratigraphic correlation and quality of the magnetic data before including these into the composite age model of the site.



175 New $\delta^{18}\text{O}_{\text{bf}}$ and $\delta^{18}\text{O}_{\text{bulk}}$ between 27–40 meter below sea floor (mbsf) correlates well with colour reflectance, whereby low/high
 $\delta^{18}\text{O}$ correlates to high/low lightness of the sediment (Fig. 3). Both show a conspicuous trough at 35.0–35.5 mbsf, and based
on the available biostratigraphic age model constraints, we interpret that to reflect the MIS M2. Tuning the resulting $\delta^{18}\text{O}_{\text{bf}}$
and colour reflectance record (Exon et al., 2001) to the CENOGRID and LR04 global stacks (Lisiecki and Raymo, 2005;
Westerhold et al., 2020) resulted in 4 solid age tie points and confidence in the stratigraphic position of the M2 isotope
180 excursion. A maximum in $\delta^{18}\text{O}_{\text{bulk}}$ at 30 mbsf is tuned to MIS G20. Additional 2 stratigraphic tie points were chosen by tuning
the colour reflectance record to CENOGRID/LR04 stack further up and down-section. See Table 1 for the stratigraphic tie
points in this paper, and the resulting age model.



185 **Figure 3: Age tuning of Pliocene Site 1168A. (a) L^* colour reflectance of Site 1168A (Exon et al., 2001). (b) $\delta^{18}\text{O}_{\text{bf}}$ and $\delta^{18}\text{O}_{\text{bulk}}$ of Site 1168A, (c) CENOGRID (Westerhold et al., 2020) and obliquity insolation curve (Laskar et al., 2004). Orange dashed lines=tie points**



Table 1: Datums of the late-Pliocene Site 1168A. Tie points as indicated in Fig. 3.

Number	Datum type	Hole	Remark	Age (ka)	Depth (mbsf)	Source
1	Colour reflectance	1168A	G17	2940	28.5	This study
2	$\delta^{18}\text{O}_{\text{bulk}}$	1168A	G20	3008.4	29.99	This study
3	$\delta^{18}\text{O}_{\text{bf}}$	1168A	KM2	3146.82	32.77	This study
4	$\delta^{18}\text{O}_{\text{bf}}$	1168A	M1	3248	34.225	This study
5	$\delta^{18}\text{O}_{\text{bf}}$	1168A	M2	3298	35.2	This study
6	$\delta^{18}\text{O}_{\text{bf}}$	1168A	MG1	3324	36.235	This study
7	$\delta^{18}\text{O}_{\text{bulk}}$	1168A	MG3	3364.6	36.80	This study

3.2 Sea surface temperature

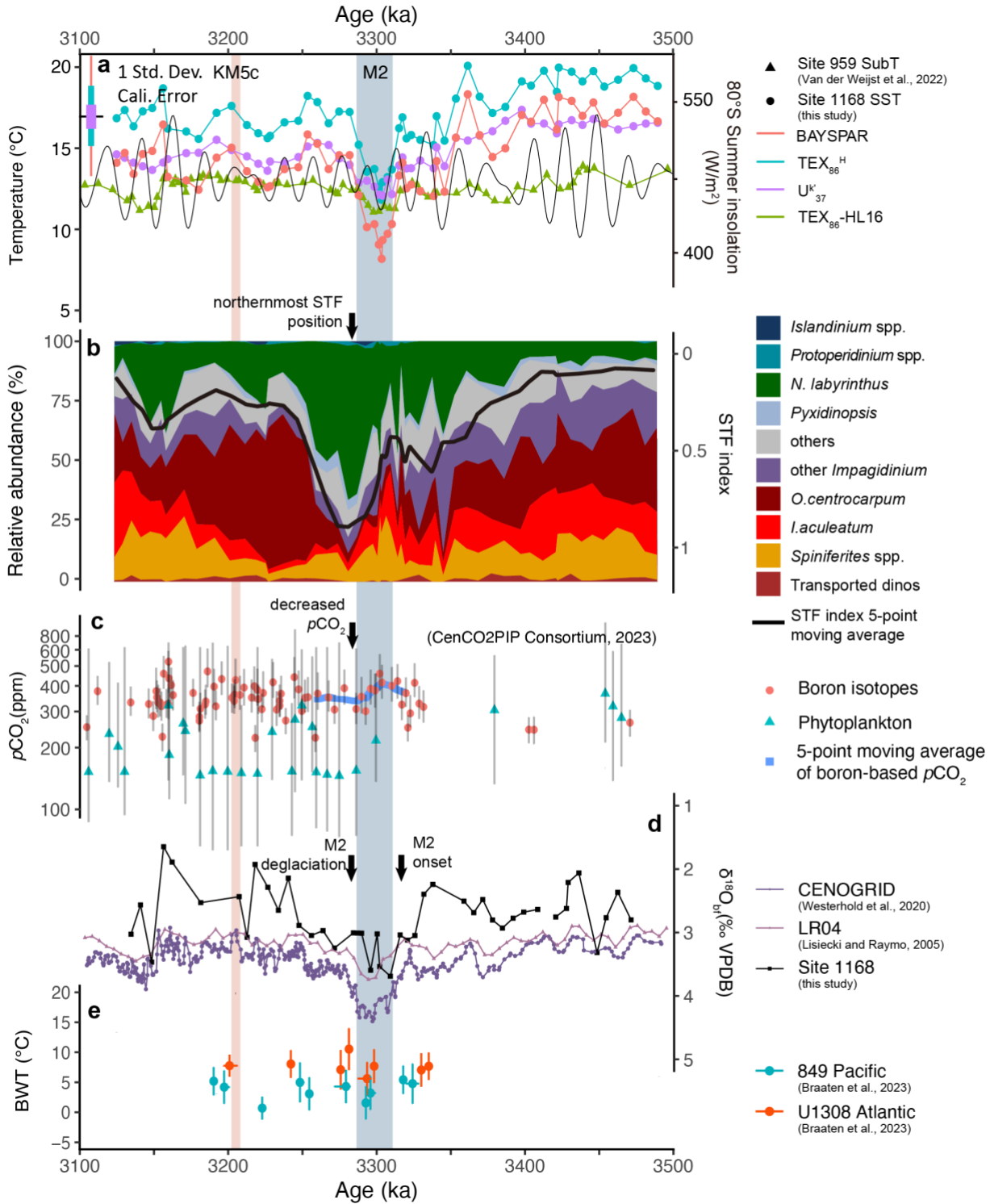
SST records of the Pliocene Site 1168 have been previously published (Hou et al., 2023a). SST proxies, U^k_{37} and TEX_{86} , were
190 calculated based on alkenones and Glycerol Dialkyl Glycerol Tetraethers (GDGTs) respectively. U^k_{37} -based SSTs vary around
17 °C prior to M2. They decrease to 12°C at the peak of the M2 glaciation (Fig. 4a). In the mPWP, SST varies around 14 °C,
which is approximately 2°C lower than the pre-M2 interval (Fig. 4a). Additionally, SST at KM5c yields 14.5 °C. TEX_{86} -based
SSTs in general resemble those derived from U^k_{37} , however, the amplitude of cooling at M2 is 3°C higher, which we cannot
195 ascribe to confounding factors in TEX_{86} : GDGT-2/GDGT-3 ratios, a general indicator for additional deep-water contributions
to TEX_{86} (Taylor et al., 2013; Ho and Laepple, 2016; van der Weijst et al., 2022), do not change across the M2 phase.

3.3 Dinocyst assemblage

Pliocene dinocyst assemblages at Site 1168 are broadly similar to modern assemblages around the subtropical front, thus enable
us to use the information of modern affinities of these species (Thöle et al., 2023) to reconstruct paleoceanographic conditions
at this site. Prior to 3400 ka, the STF index is about 0.3 and assemblages are typical for modern regions north of the STF (Fig.



200 4b), with abundant *O.centrocarpum* (High-Ocen-cluster), *I.aculeatum* (Iacu cluster) and *Spiniferites* spp (Spin-cluster; Thöle
et al., 2023). The increase of *N. labyrinthus* (around 3400 ka) makes the assemblages progressively more similar to those of
the SAZ, south of the STF and forms the Nlab-cluster when it is dominant in the assemblage (>40%). The attendance of *I.*
pallidum is sporadic throughout the record, however, transiently increases to ~10% at 3300ka and dominates the other
Impagidinium group (see raw data). The abundance of *N. labyrinthus* peaks at 3275 ka and the STF index reaches 0.8, well
205 after the peak of the M2, in the M2 deglaciation stage (Fig. 4b). Thereafter, north-of-STF assemblages recovered and replaced
N. labyrinthus in the mPWP.





210 **Figure 4: Late-Pliocene proxy compilation for oceanographic change at ODP Site 1168, and published $p\text{CO}_2$, BWT reconstructions.**
(a) Sea surface temperature at Site 1168 based on TEX_{86} (exponential $\text{TEX}_{86}^{\text{H}}$ and BAYSPAR calibrations; Kim et al., 2010; Tierney
and Tingley, 2014) and U^k_{37} (linear calibration; Müller et al., 1998). Subsurface temperature at Site 959 (Van der Weijst et al., 2022)
using the HL-16 calibration (Ho and Laepple, 2016). Antarctic summer (80°S January) insolation on the second y-axis (Laskar et
al., 2004; de Boer et al., 2014). (b) Dinocyst assemblages of Site 1168, green = south of STF species, orange, red and burgundy =
north of STF species, petrol and blue = high productivity and/or sea ice affiliated species (Thöle et al., 2023). Black line represents a
215 5-point moving average of dinocyst-based STF index (South of STF/(South+North of STF)) roughly indicating the position of the STF
at ODP Site 1168 that we derive from these dinocysts assemblages (up or 0 is north, down or 1 is south position). (c) $p\text{CO}_2$ derived
from boron isotopes (red dots) and alkenone $\delta^{13}\text{C}$ (cyan triangles) (CENCO2PIP CONSORTIUM, 2023 and references therein) and
a 5-point moving average record based on boron isotopes (blue curve); vertical error bar=95% confidence interval. (d) Benthic
foraminiferal $\delta^{18}\text{O}$ of ODP Site 1168 and global stacks (Lisiecki and Raymo, 2005; Westerhold et al., 2020). (e) Bottom water
220 temperature of ODP Site 849 (blue dots) and IODP Site U1308 (orange dots, Braaten et al., 2023), vertical error bar=95% confidence
interval, horizontal error bar= averaged age range.

4 Discussion

4.1 STF migrations and SAZ surface conditions in the late Pliocene

Lowest local SSTs (13°C based on U^k_{37}) were recorded at peak M2 glaciation: $\sim 6^\circ\text{C}$ lower than those before M2 and $\sim 5^\circ\text{C}$
lower than those in the mPWP (Fig. 4a). The amplitude of the SST variation over the mPWP glacial-interglacial cycles is about
225 $1\text{--}2^\circ\text{C}$, much smaller than the cooling associated with M2. In terms of the cooling amplitude, SSTs in low–mid latitudes
during M2 suggest that it represents an unusual strong glacial (Lawrence et al., 2009; De Schepper et al., 2013; Liu et al., 2019,
2022; van der Weijst et al., 2022). However, SST reconstructions from high latitude surface (Risebrobakken et al., 2016;
Bachem et al., 2017) and deep ocean (Braaten et al., 2023) suggest that either the M2 indicates no profound cooling, or the
cooling has similar amplitude as other glacial phases within the mPWP. The extreme SST response to M2 in the subantarctic
230 zone is therefore extraordinary, and perhaps not the result of radiative forcing but amplified by regional or local oceanographic
changes. Furthermore, SSTs of Site 1168 are highly consistent with the subsurface temperature of Site 959 recording South
Atlantic Central Water, which derives from the Southern Hemisphere subtropical surface ocean (SACW, van der Weijst et al.,
2022). Therefore, their similarity to surface temperatures at Site 1168 is not surprising.

235 The dinocyst assemblage indicate that the most northern position of the STF is reached during the M2–mPWP transition, i.e.
when SST at ODP Site 1168 increased over 5°C (Fig. 4a, b). Both peak M2 and M2 deglaciation SSTs at 1168 are within the
modern SST range of Nlab-cluster (Fig. 2), although the $15\text{--}17^\circ\text{C}$ (both proxies) at deglaciation does approach the upper limit
of the SST range of Nlab-cluster (Fig. 2b; Thöle et al., 2023). Based on the modern dinocyst distributions (Fig. 2b), and in
particular the proliferation of *N. labyrinthus* (Fig. 4b), the surface ocean became ~ 1.5 psu fresher during the M2 deglaciation.
240 Since there is no evidence in the palynological slides nor in GDGT-based indices (Hou et al., 2023a) for enhanced terrestrial
input from runoff, we conclude that the surface ocean freshening of the subantarctic zone at M2 deglaciation originated from
excessive iceberg discharge, which melted in the SAZ.



Overall, according to the changes we observed in dinocyst assemblages, we estimate that the STF was positioned to the south
245 of Site 1168 from prior to M2 until its onset; the STF moved northward as SST decreased and *N.labyrinthus* increased during
M2; During the recovery of M2, the STF moved further northward and approached the margin of Tasmania (42°S) at 3275 ka,
and surface waters strongly freshened. During the mPWP, the surface salinity at Site 1168 normalized and the STF shifted
poleward to a similar position as before M2.

250 **4.2 Southern Ocean carbon outgassing as $p\text{CO}_2$ regulator across M2**

By comparing our reconstructed STF migrations with the available $p\text{CO}_2$ reconstructions across the M2 event, we note a
coincidence in phase, much stronger than with SST or benthic $\delta^{18}\text{O}$ changes (that do correlate well with each other). In other
words, frontal shifts and $p\text{CO}_2$ lag SST and benthic $\delta^{18}\text{O}$ across M2. The bulk of the late Pliocene $p\text{CO}_2$ record is generated
from ODP Site 999, of which the surface air-sea disequilibrium for CO_2 is close to 0 (Martínez-Botí et al., 2015). Thus, this
255 Caribbean Sea site has been frequently used to reconstruct global past $p\text{CO}_2$ (Foster, 2008; Chalk et al., 2017; De la Vega et
al., 2020, 2023).

At the onset of M2, $p\text{CO}_2$ was about 400 ppm (De la Vega et al., 2020) and Site 1168 had an abundance of warm species
suggesting a southerly position of the STF. Following this maximum, the STF was moving northwards during the M2 $\delta^{18}\text{O}$
260 peak and the coolest SSTs (Fig. 4a). However, The STF reached its northernmost position at the deglaciation phase of M2
event, and this corresponds to the lowest $p\text{CO}_2$ (Fig. 4c). During the mPWP, when SST was high, the STF migrated back
southward and $p\text{CO}_2$ gradually increased to ~400 ppm. We deduce from this correlation that the oceanographic changes in the
SAZ influenced the ocean uptake efficiency of atmospheric carbon, which had an effect on $p\text{CO}_2$, but that this occurred out of
phase with the temperature and benthic $\delta^{18}\text{O}$ changes. The mechanism we propose involves the ocean as source and sink of
265 atmospheric CO_2 and the shifting fronts and sea ice.

The migrations of the STF in the Tasmanian sector are the consequences of the shifts in westerlies and Antarctic-proximal sea
ice extent – in the Pleistocene and Miocene (Groeneveld et al., 2017; Kohfeld and Chase, 2017; Hou et al., 2023b) but also in
the Pliocene. During the M2, the STF gradually shifted northward, indicating an equivalent shift of the westerlies and a
270 northward expansion of the subantarctic zone. The northward migration of the westerlies and fronts enhanced the stratification
of the Southern Ocean and thereby prevented respired CO_2 from outgassing into the atmosphere. Consequently, $p\text{CO}_2$ dropped,
in phase with the northward migration of the STF. At the same time, the freshening of the surface SAZ (Fig. 1) must have
lowered carbon uptake in the surface ocean (Bourgeois et al., 2022). However, the decreased $p\text{CO}_2$ apparently suggests that
the lowered surface carbon uptake did not compensate for the reduction of emission induced by the expanding sea ice cover
275 in the polar frontal zone. The equatorward shift of the STF, which continued into the deglaciation stage of the M2, was
associated with expanded sea ice cover in the polar frontal zone, especially in the deglaciation stage, when surface waters



freshened. The higher amplitude of obliquity increased Antarctic summer insolation after M2 peak glacial advance (Fig. 4a) and this probably enhanced iceberg calving, which stimulated the northward migration and freshening of STF. Furthermore, Antarctic ice sheet simulations suggest that insolation-driven sub-shelf melting can be linked to changes in the carbon
280 cycle (De Boer et al., 2014). Indeed, massive iceberg calving was noticed at the east Antarctic margin during deglacials in the Pliocene, associated with maximum iceberg-rafted debris (Cook et al., 2013; Patterson et al., 2014), which is in line with our frontal migration record.

When the M2 deglaciation was complete, in the mPWP, iceberg discharge ceased (Patterson et al., 2014) because in the sector
285 of Antarctica nearest to our site fewer glaciers terminated in the ocean (Cook et al., 2013), sea ice cover decreased (Patterson et al., 2014), and westerlies moved southward. As such, the patterns in sea ice cover over the polar front controlled air-sea gas exchange: the weaker the sea ice cover, the less stratification, the more CO₂ outgassing from the CO₂-rich deep water. Similar mechanisms, involving sea ice cover as regulator for Southern Ocean air-sea CO₂ exchange, have been proposed for the Pleistocene and Quaternary (Sigman et al., 2010; Kohfeld and Chase, 2017). Furthermore, the dinocyst-based, poleward
290 positioned STF in the mPWP fell in line with simulated weak stratification and enhanced outgassing in the Southern Ocean (Zhang et al., 2013), which resulted in elevated *p*CO₂. However, new PlioMIP2 models yield contradictory results (Weiffenbach et al., 2023). Simulations on the Southern Ocean thus are highly model dependent (Zhang et al., 2021; Weiffenbach et al., 2023). In any case, present models are not able to resolve frontal migrations or local effects due to their spatial resolution.

295 Nevertheless, *p*CO₂ in the Pleistocene (Bereiter et al., 2015; Yan et al., 2019) does not show lags between surface oceanography and benthic δ¹⁸O changes (Lisiecki and Raymo, 2005; Martínez-García et al., 2010; Chalk et al., 2017) as much as the M2-mPWP interval shows here. Shifts in westerlies further drove variations of dust input to the Pleistocene ocean (Abell et al., 2021) and influenced CO₂ uptake through the biological carbon pump (Thöle et al., 2019). Essentially, its impact on carbon
300 storage was in phase with deep ocean CO₂ degassing, e.g., inducing lower *p*CO₂ in the Pleistocene glacial maxima (Ziegler et al., 2013; Ai et al., 2020). However, late-Pliocene aeolian input was limited both regionally in the Southern Ocean (Martínez-García et al., 2010; Naafs et al., 2012) and globally (Teruel et al., 2021), and therefore this process played a less important role during the Pliocene. M2 glaciation occurred mainly as orbital-forced ice buildup and did not seem to have been triggered by a decline in *p*CO₂ (De la Vega et al., 2020). A new study of Δ₄₇-based BWTs in the north Atlantic and north Pacific has found
305 that deep sea cooling lags the positive δ¹⁸O excursion of M2 by ~20kyrs (Fig. 4d, e; Braaten et al., 2023), but is in phase with the *p*CO₂ variations (De la Vega et al., 2020). Therefore, moderate changes in Pliocene *p*CO₂ across the M2 were independent of global ice volume change but instead linked to oceanographic changes (including deep ocean temperature) through the *p*CO₂-global climate positive feedback (Braaten et al., 2023).



5 Conclusions

310 Our new Pliocene dinocyst assemblage data combined with previously published SSTs from the same site shed new light on
the dynamics of Southern Ocean frontal systems, in relation to ice sheet and sea ice. We reconstruct that the STF migrated
substantially across the M2–mPWP climatic transition. Vast sea ice extent and iceberg discharge during the deglaciation stage
of M2 pushed the STF to its northernmost position, freshened it, and prevented respired CO₂ emissions from the deep ocean
to the atmosphere. This suggests that, across the M2 event, Southern Ocean frontal migrations controlled ocean-air CO₂
315 exchange and resulted in the *p*CO₂ changes on orbital timescales.

Data availability

The new palynological and benthic and bulk stable isotope data from Site 1168 are deposited at Zenodo
<https://doi.org/10.5281/zenodo.11086278>. All other data presented have been deposited already, and references to those
repository items can be found in the respective publications.

320 Author contributions

PKB designed the research. SH and LT processed and analysed samples for palynology, SH and PKB interpreted the
palynological results. SH and MvdL washed and picked benthic foraminifera and generated the stable and clumped isotopes
data. FR measured the bulk carbonate isotopes. SH, LJJ and PKB refined the age model. SH wrote the paper with input from
PKB, LJJ and MZ. All authors have contributed to the submitted manuscript.

325 Competing interests

The contact author declares no competing interests.

Acknowledgements

We thank Mariska Hoorweg, Natasja Welters, Giovanni Dammers, Desmond Eefting and Arnold van Dijk for laboratory
assistance. We thank IODP and scientists of ODP Leg 189, and technicians at KCC in Kochi, Japan for making samples and
330 data available. We are grateful to Lena Thöle, Julia Weiffenbach and Anna Braaten for discussions, and the latter also for
providing revised clumped isotope data. This research is funded by ERC Starting Grant 802835 to Peter K. Bijl.



References

- Abell, J. T., Winckler, G., Anderson, R. F., and Herbert, T. D.: Poleward and weakened westerlies during Pliocene warmth, *Nature*, 589, 70–75, <https://doi.org/10.1038/s41586-020-03062-1>, 2021.
- 335 Acker, J. G. and Leptoukh, G.: Online analysis enhances use of NASA Earth science data, *Eos, Transactions American Geophysical Union*, 88, 14–17, <https://doi.org/10.1029/2007EO020003>, 2007.
- Ai, X. E., Studer, A. S., Sigman, D. M., Martínez-García, A., Fripiat, F., Thöle, L. M., Michel, E., Gottschalk, J., Arnold, L., Moretti, S., Schmitt, M., Oleynik, S., Jaccard, S. L., and Haug, G. H.: Southern Ocean upwelling, Earth’s obliquity, and glacial-interglacial atmospheric CO₂ change, *Science*, 370, 1348–1352, <https://doi.org/10.1126/science.abd2115>, 2020.
- 340 Bachem, P. E., Risebrobakken, B., De Schepper, S., and McClymont, E. L.: Highly variable Pliocene sea surface conditions in the Norwegian Sea, *Climate of the Past*, 13, 1153–1168, <https://doi.org/10.5194/cp-13-1153-2017>, 2017.
- Bereiter, B., Eggleston, S., Schmitt, J., Nehrbass-Ahles, C., Stocker, T. F., Fischer, H., Kipfstuhl, S., and Chappellaz, J.: Revision of the EPICA Dome C CO₂ record from 800 to 600 kyr before present, *Geophysical Research Letters*, 42, 542–549, <https://doi.org/10.1002/2014GL061957>, 2015.
- 345 Bijl, P. K. and Brinkhuis, H.: Palsys.org: an open-access taxonomic and stratigraphic database of organic-walled dinoflagellate cysts, *Journal of Micropalaeontology*, 42, 309–314, <https://doi.org/10.5194/jm-42-309-2023>, 2023.
- de Boer, B., Lourens, L. J., and van de Wal, R. S. W.: Persistent 400,000-year variability of Antarctic ice volume and the carbon cycle is revealed throughout the Plio-Pleistocene, *Nat Commun*, 5, 2999, <https://doi.org/10.1038/ncomms3999>, 2014.
- Bourgeois, T., Goris, N., Schwinger, J., and Tjiputra, J. F.: Stratification constrains future heat and carbon uptake in the Southern Ocean between 30°S and 55°S, *Nat Commun*, 13, 340, <https://doi.org/10.1038/s41467-022-27979-5>, 2022.
- 350 Brinkhuis, H., Munsterman, D. K., Sengers, M. J., Sluijs, A., Warnaar, J., and Williams, G. L.: LATE EOCENE–QUATERNARY DINOFLAGELLATE CYSTS FROM ODP SITE 1168, OFF WESTERN TASMANIA, *Ocean Drilling Program*, <https://doi.org/10.2973/odp.proc.sr.189.2004>, 2004.
- Burton, L. E., Haywood, A. M., Tindall, J. C., Dolan, A. M., Hill, D. J., Abe-Ouchi, A., Chan, W.-L., Chandan, D., Feng, R., Hunter, S. J., Li, X., Peltier, W. R., Tan, N., Stepanek, C., and Zhang, Z.: On the climatic influence of CO₂ forcing in the Pliocene, *Climate of the Past*, 19, 747–764, <https://doi.org/10.5194/cp-19-747-2023>, 2023.
- 355 CENCO2PIP CONSORTIUM: Toward a Cenozoic history of atmospheric CO₂, *Science*, 382, eadi5177, <https://doi.org/10.1126/science.adi5177>, 2023.
- Chalk, T. B., Hain, M. P., Foster, G. L., Rohling, E. J., Sexton, P. F., Badger, M. P. S., Cherry, S. G., Hasenfratz, A. P., Haug, G. H., Jaccard, S. L., Martínez-García, A., Pälike, H., Pancost, R. D., and Wilson, P. A.: Causes of ice age intensification across the Mid-Pleistocene Transition, *Proceedings of the National Academy of Sciences*, 114, 13114–13119, <https://doi.org/10.1073/pnas.1702143114>, 2017.
- Cook, C. P., van de Flierdt, T., Williams, T., Hemming, S. R., Iwai, M., Kobayashi, M., Jimenez-Espejo, F. J., Escutia, C., González, J. J., Khim, B.-K., McKay, R. M., Passchier, S., Bohaty, S. M., Riesselman, C. R., Tauxe, L., Sugisaki, S., Galindo,



- 365 A. L., Patterson, M. O., Sangiorgi, F., Pierce, E. L., Brinkhuis, H., Klaus, A., Fehr, A., Bendle, J. A. P., Bijl, P. K., Carr, S. A., Dunbar, R. B., Flores, J. A., Hayden, T. G., Katsuki, K., Kong, G. S., Nakai, M., Olney, M. P., Pekar, S. F., Pross, J., Röhl, U., Sakai, T., Shrivastava, P. K., Stickley, C. E., Tuo, S., Welsh, K., and Yamane, M.: Dynamic behaviour of the East Antarctic ice sheet during Pliocene warmth, *Nature Geosci*, 6, 765–769, <https://doi.org/10.1038/ngeo1889>, 2013.
- De la Vega, E., Chalk, T. B., Wilson, P. A., Bysani, R. P., and Foster, G. L.: Atmospheric CO₂ during the Mid-Piacenzian
370 Warm Period and the M2 glaciation, *Sci Rep*, 10, 11002, <https://doi.org/10.1038/s41598-020-67154-8>, 2020.
- De la Vega, E., Chalk, T. B., Hain, M. P., Wilding, M. R., Casey, D., Gledhill, R., Luo, C., Wilson, P. A., and Foster, G. L.: Orbital CO₂ reconstruction using boron isotopes during the late Pleistocene, an assessment of accuracy, *Climate of the Past*, 19, 2493–2510, <https://doi.org/10.5194/cp-19-2493-2023>, 2023.
- De Schepper, S., Fischer, E. I., Groeneveld, J., Head, M. J., and Matthiessen, J.: Deciphering the palaeoecology of Late
375 Pliocene and Early Pleistocene dinoflagellate cysts, *Palaeogeography, Palaeoclimatology, Palaeoecology*, 309, 17–32, <https://doi.org/10.1016/j.palaeo.2011.04.020>, 2011.
- De Schepper, S., Groeneveld, J., Naafs, B. D. A., Van Renterghem, C., Hennissen, J., Head, M. J., Louwye, S., and Fabian, K.: Northern Hemisphere Glaciation during the Globally Warm Early Late Pliocene, *PLoS ONE*, 8, e81508, <https://doi.org/10.1371/journal.pone.0081508>, 2013.
- 380 Egleston, E. S., Sabine, C. L., and Morel, F. M. M.: Revelle revisited: Buffer factors that quantify the response of ocean chemistry to changes in DIC and alkalinity, *Global Biogeochemical Cycles*, 24, <https://doi.org/10.1029/2008GB003407>, 2010.
- Exon, N. F., Kennett, J. P., and Malone, M. J.: Ocean Drilling Program Leg 189 Initial Reports: Chapter 3, 2001.
- Flesche Kleiven, H., Jansen, E., Fronval, T., and Smith, T. M.: Intensification of Northern Hemisphere glaciations in the circum Atlantic region (3.5–2.4 Ma) – ice-rafted detritus evidence, *Palaeogeography, Palaeoclimatology, Palaeoecology*, 184, 213–
385 223, [https://doi.org/10.1016/S0031-0182\(01\)00407-2](https://doi.org/10.1016/S0031-0182(01)00407-2), 2002.
- Foster, G. L.: Seawater pH, pCO₂ and [CO₂–3] variations in the Caribbean Sea over the last 130 kyr: A boron isotope and B/Ca study of planktic foraminifera, *Earth and Planetary Science Letters*, 271, 254–266, <https://doi.org/10.1016/j.epsl.2008.04.015>, 2008.
- Friedlingstein, P., O’Sullivan, M., Jones, M. W., Andrew, R. M., Gregor, L., Hauck, J., Le Quéré, C., Lujikx, I. T., Olsen, A.,
390 Peters, G. P., Peters, W., Pongratz, J., Schwingshackl, C., Sitch, S., Canadell, J. G., Ciais, P., Jackson, R. B., Alin, S. R., Alkama, R., Arneeth, A., Arora, V. K., Bates, N. R., Becker, M., Bellouin, N., Bittig, H. C., Bopp, L., Chevallier, F., Chini, L. P., Cronin, M., Evans, W., Falk, S., Feely, R. A., Gasser, T., Gehlen, M., Gkritzalis, T., Gloege, L., Grassi, G., Gruber, N., Gürses, Ö., Harris, I., Hefner, M., Houghton, R. A., Hurtt, G. C., Iida, Y., Ilyina, T., Jain, A. K., Jersild, A., Kadono, K., Kato, E., Kennedy, D., Klein Goldewijk, K., Knauer, J., Korsbakken, J. I., Landschützer, P., Lefèvre, N., Lindsay, K., Liu, J., Liu, Z., Marland, G., Mayot, N., McGrath, M. J., Metzl, N., Monacci, N. M., Munro, D. R., Nakaoka, S.-I., Niwa, Y., O’Brien, K., Ono, T., Palmer, P. I., Pan, N., Pierrot, D., Pockock, K., Poulter, B., Resplandy, L., Robertson, E., Rödenbeck, C., Rodriguez, C., Rosan, T. M., Schwinger, J., Séférian, R., Shutler, J. D., Skjelvan, I., Steinhoff, T., Sun, Q., Sutton, A. J., Sweeney, C., Takao, S., Tanhua, T., Tans, P. P., Tian, X., Tian, H., Tilbrook, B., Tsujino, H., Tubiello, F., van der Werf, G. R., Walker, A.



- P., Wanninkhof, R., Whitehead, C., Willstrand Wranne, A., et al.: Global Carbon Budget 2022, *Earth System Science Data*, 400 14, 4811–4900, <https://doi.org/10.5194/essd-14-4811-2022>, 2022.
- Groeneveld, J., Henderiks, J., Renema, W., McHugh, C. M., De Vleeschouwer, D., Christensen, B. A., Fulthorpe, C. S., Reuning, L., Gallagher, S. J., Bogus, K., Auer, G., Ishiwa, T., and Expedition 356 Scientists: Australian shelf sediments reveal shifts in Miocene Southern Hemisphere westerlies, *Sci. Adv.*, 3, e1602567, <https://doi.org/10.1126/sciadv.1602567>, 2017.
- Gruber, N., Bakker, D. C. E., DeVries, T., Gregor, L., Hauck, J., Landschützer, P., McKinley, G. A., and Müller, J. D.: Trends 405 and variability in the ocean carbon sink, *Nat Rev Earth Environ*, 4, 119–134, <https://doi.org/10.1038/s43017-022-00381-x>, 2023.
- Han, Z., Zhang, Q., Li, Q., Feng, R., Haywood, A. M., Tindall, J. C., Hunter, S. J., Otto-Bliesner, B. L., Brady, E. C., Rosenbloom, N., Zhang, Z., Li, X., Guo, C., Nisancioglu, K. H., Stepanek, C., Lohmann, G., Sohl, L. E., Chandler, M. A., Tan, N., Ramstein, G., Baatsen, M. L. J., von der Heydt, A. S., Chandan, D., Peltier, W. R., Williams, C. J. R., Lunt, D. J., 410 Cheng, J., Wen, Q., and Burls, N. J.: Evaluating the large-scale hydrological cycle response within the Pliocene Model Intercomparison Project Phase 2 (PliMIP2) ensemble, *Climate of the Past*, 17, 2537–2558, <https://doi.org/10.5194/cp-17-2537-2021>, 2021.
- Haywood, A. M., Tindall, J. C., Dowsett, H. J., Dolan, A. M., Foley, K. M., Hunter, S. J., Hill, D. J., Chan, W.-L., Abe-Ouchi, A., Stepanek, C., Lohmann, G., Chandan, D., Peltier, W. R., Tan, N., Contoux, C., Ramstein, G., Li, X., Zhang, Z., Guo, C., 415 Nisancioglu, K. H., Zhang, Q., Li, Q., Kamae, Y., Chandler, M. A., Sohl, L. E., Otto-Bliesner, B. L., Feng, R., Brady, E. C., von der Heydt, A. S., Baatsen, M. L. J., and Lunt, D. J.: The Pliocene Model Intercomparison Project Phase 2: large-scale climate features and climate sensitivity, *Climate of the Past*, 16, 2095–2123, <https://doi.org/10.5194/cp-16-2095-2020>, 2020.
- Heath, R. A.: A review of the physical oceanography of the seas around New Zealand — 1982, *New Zealand Journal of Marine and Freshwater Research*, 19, 79–124, <https://doi.org/10.1080/00288330.1985.9516077>, 1985.
- 420 Ho, S. L. and Laepple, T.: Flat meridional temperature gradient in the early Eocene in the subsurface rather than surface ocean, *Nature Geosci*, 9, 606–610, <https://doi.org/10.1038/ngeo2763>, 2016.
- Hou, S., Lamprou, F., Hoem, F. S., Hadju, M. R. N., Sangiorgi, F., Peterse, F., and Bijl, P. K.: Lipid-biomarker-based sea surface temperature record offshore Tasmania over the last 23 million years, *Climate of the Past*, 19, 787–802, <https://doi.org/10.5194/cp-19-787-2023>, 2023a.
- 425 Hou, S., Stap, L. B., Paul, R., Nelissen, M., Hoem, F. S., Ziegler, M., Sluijs, A., Sangiorgi, F., and Bijl, P. K.: Reconciling Southern Ocean fronts equatorward migration with minor Antarctic ice volume change during Miocene cooling, *Nat Commun*, 14, 7230, <https://doi.org/10.1038/s41467-023-43106-4>, 2023b.
- IPCC: Special Report on the Ocean and Cryosphere in a Changing Climate —, 2019.
- Keigwin, L.: PLIOCENE STABLE-ISOTOPE RECORD OF DEEP SEA DRILLING PROJECT SITE 606: SEQUENTIAL 430 EVENTS OF 18O ENRICHMENT BEGINNING AT 3.1 MA, U.S. Government Printing Office, <https://doi.org/10.2973/dsdp.proc.94.1987>, 1987.



- Kim, J.-H., van der Meer, J., Schouten, S., Helmke, P., Willmott, V., Sangiorgi, F., Koç, N., Hopmans, E. C., and Damsté, J. S. S.: New indices and calibrations derived from the distribution of crenarchaeal isoprenoid tetraether lipids: Implications for past sea surface temperature reconstructions, *Geochimica et Cosmochimica Acta*, 74, 4639–4654, 435 <https://doi.org/10.1016/j.gca.2010.05.027>, 2010.
- Kocken, I. J., Müller, I. A., and Ziegler, M.: Optimizing the Use of Carbonate Standards to Minimize Uncertainties in Clumped Isotope Data, *Geochemistry, Geophysics, Geosystems*, 20, 5565–5577, <https://doi.org/10.1029/2019GC008545>, 2019.
- Kohfeld, K. E. and Chase, Z.: Temporal evolution of mechanisms controlling ocean carbon uptake during the last glacial cycle, *Earth and Planetary Science Letters*, 472, 206–215, <https://doi.org/10.1016/j.epsl.2017.05.015>, 2017.
- 440 Lawrence, K. T., Herbert, T. D., Brown, C. M., Raymo, M. E., and Haywood, A. M.: High-amplitude variations in North Atlantic sea surface temperature during the early Pliocene warm period, *Paleoceanography*, 24, <https://doi.org/10.1029/2008PA001669>, 2009.
- Lisiecki, L. E. and Raymo, M. E.: A Pliocene-Pleistocene stack of 57 globally distributed benthic $\delta^{18}\text{O}$ records: PLIOCENE-PLEISTOCENE BENTHIC STACK, *Paleoceanography*, 20, n/a-n/a, <https://doi.org/10.1029/2004PA001071>, 2005.
- 445 Liu, J., Tian, J., Liu, Z., Herbert, T. D., Fedorov, A. V., and Lyle, M.: Eastern equatorial Pacific cold tongue evolution since the late Miocene linked to extratropical climate, *Sci. Adv.*, 5, eaau6060, <https://doi.org/10.1126/sciadv.aau6060>, 2019.
- Liu, X., Huber, M., Foster, G. L., Dessler, A., and Zhang, Y. G.: Persistent high latitude amplification of the Pacific Ocean over the past 10 million years, *Nat Commun*, 13, 7310, <https://doi.org/10.1038/s41467-022-35011-z>, 2022.
- Martin, J. H.: Glacial-interglacial CO_2 change: The Iron Hypothesis, *Paleoceanography*, 5, 1–13, 450 <https://doi.org/10.1029/PA005i001p00001>, 1990.
- Martínez-Botí, M. A., Foster, G. L., Chalk, T. B., Rohling, E. J., Sexton, P. F., Lunt, D. J., Pancost, R. D., Badger, M. P. S., and Schmidt, D. N.: Plio-Pleistocene climate sensitivity evaluated using high-resolution CO_2 records, *Nature*, 518, 49–54, <https://doi.org/10.1038/nature14145>, 2015.
- Martínez-García, A., Rosell-Melé, A., McClymont, E. L., Gersonde, R., and Haug, G. H.: Subpolar Link to the Emergence of 455 the Modern Equatorial Pacific Cold Tongue, *Science*, 328, 1550–1553, <https://doi.org/10.1126/science.1184480>, 2010.
- Martínez-García, A., Sigman, D. M., Ren, H., Anderson, R. F., Straub, M., Hodell, D. A., Jaccard, S. L., Eglinton, T. I., and Haug, G. H.: Iron Fertilization of the Subantarctic Ocean During the Last Ice Age, *Science*, 343, 1347–1350, <https://doi.org/10.1126/science.1246848>, 2014.
- Mas e Braga, M., Jones, R. S., Bernales, J., Andersen, J. L., Fredin, O., Morlighem, M., Koester, A. J., Lifton, N. A., Harbor, 460 J. M., Sugauma, Y., Glasser, N. F., Rogozhina, I., and Stroeven, A. P.: A thicker Antarctic ice stream during the mid-Pliocene warm period, *Commun Earth Environ*, 4, 1–13, <https://doi.org/10.1038/s43247-023-00983-3>, 2023.
- McClymont, E. L., Ford, H. L., Ho, S. L., Tindall, J. C., Haywood, A. M., Alonso-Garcia, M., Bailey, I., Berke, M. A., Littler, K., Patterson, M. O., Petrick, B., Peterse, F., Ravelo, A. C., Risebrobakken, B., De Schepper, S., Swann, G. E. A., Thirumalai, K., Tierney, J. E., van der Weijst, C., White, S., Abe-Ouchi, A., Baatsen, M. L. J., Brady, E. C., Chan, W.-L., Chandan, D., 465 Feng, R., Guo, C., von der Heydt, A. S., Hunter, S., Li, X., Lohmann, G., Nisancioglu, K. H., Otto-Bliesner, B. L., Peltier, W.



- R., Stepanek, C., and Zhang, Z.: Lessons from a high-CO₂ world: an ocean view from ~ 3 million years ago, *Clim. Past*, 16, 1599–1615, <https://doi.org/10.5194/cp-16-1599-2020>, 2020.
- McKay, R., Naish, T., Carter, L., Riesselman, C., Dunbar, R., Sjunneskog, C., Winter, D., Sangiorgi, F., Warren, C., Pagani, M., Schouten, S., Willmott, V., Levy, R., DeConto, R., and Powell, R. D.: Antarctic and Southern Ocean influences on Late Pliocene global cooling, *Proc. Natl. Acad. Sci. U.S.A.*, 109, 6423–6428, <https://doi.org/10.1073/pnas.1112248109>, 2012.
- Müller, P. J., Kirst, G., Ruhland, G., von Storch, I., and Rosell-Melé, A.: Calibration of the alkenone paleotemperature index U37K' based on core-tops from the eastern South Atlantic and the global ocean (60°N–60°S), *Geochimica et Cosmochimica Acta*, 62, 1757–1772, [https://doi.org/10.1016/S0016-7037\(98\)00097-0](https://doi.org/10.1016/S0016-7037(98)00097-0), 1998.
- Naafs, B. D. A., Hefter, J., Acton, G., Haug, G. H., Martínez-García, A., Pancost, R., and Stein, R.: Strengthening of North American dust sources during the late Pliocene (2.7Ma), *Earth and Planetary Science Letters*, 317–318, 8–19, <https://doi.org/10.1016/j.epsl.2011.11.026>, 2012.
- Patterson, M. O., McKay, R., Naish, T., Escutia, C., Jimenez-Espejo, F. J., Raymo, M. E., Meyers, S. R., Tauxe, L., and Brinkhuis, H.: Orbital forcing of the East Antarctic ice sheet during the Pliocene and Early Pleistocene, *Nature Geosci*, 7, 841–847, <https://doi.org/10.1038/ngeo2273>, 2014.
- Rae, J. W. B., Burke, A., Robinson, L. F., Adkins, J. F., Chen, T., Cole, C., Greenop, R., Li, T., Littley, E. F. M., Nita, D. C., Stewart, J. A., and Taylor, B. J.: CO₂ storage and release in the deep Southern Ocean on millennial to centennial timescales, *Nature*, 562, 569–573, <https://doi.org/10.1038/s41586-018-0614-0>, 2018.
- Risebrobakken, B., Andersson, C., De Schepper, S., and McClymont, E. L.: Low-frequency Pliocene climate variability in the eastern Nordic Seas, *Paleoceanography*, 31, 1154–1175, <https://doi.org/10.1002/2015PA002918>, 2016.
- Sabine, C. L., Feely, R. A., Gruber, N., Key, R. M., Lee, K., Bullister, J. L., Wanninkhof, R., Wong, C. S., Wallace, D. W. R., Tilbrook, B., Millero, F. J., Peng, T.-H., Kozyr, A., Ono, T., and Rios, A. F.: The Oceanic Sink for Anthropogenic CO₂, *Science*, 305, 367–371, <https://doi.org/10.1126/science.1097403>, 2004.
- Shackleton, N. J., Hall, M. A., and Pate: Proceedings of the Ocean Drilling Program, 138 Scientific Results, Ocean Drilling Program, <https://doi.org/10.2973/odp.proc.sr.138.1995>, 1995.
- Sigman, D. M., Hain, M. P., and Haug, G. H.: The polar ocean and glacial cycles in atmospheric CO₂ concentration, *Nature*, 466, 47–55, <https://doi.org/10.1038/nature09149>, 2010.
- Skinner, L. C., Fallon, S., Waelbroeck, C., Michel, E., and Barker, S.: Ventilation of the Deep Southern Ocean and Deglacial CO₂ Rise, *Science*, 328, 1147–1151, <https://doi.org/10.1126/science.1183627>, 2010.
- Stickley, C. E., Fuller, M., Kelly, D. C., Nürnberg, D., Pfuhl, H. A., Schellenberg, S. A., Schoenfeld, J., Suzuki, N., Touchard, Y., Wei, W., Williams, G. L., Lara, J., and Stant, S. A.: Proceedings of the Ocean Drilling Program, 189 Scientific Results, edited by: Exon, N. F., Kennett, J. P., and Malone, M. J., Ocean Drilling Program, <https://doi.org/10.2973/odp.proc.sr.189.2004>, 2004.
- Stockmarr, J.: Tables with spores used in absolute pollen analysis, *Pollen et Spores*, 13, 615–621, 1971.



- Taylor, K. W. R., Huber, M., Hollis, C. J., Hernandez-Sanchez, M. T., and Pancost, R. D.: Re-evaluating modern and
500 Palaeogene GDGT distributions: Implications for SST reconstructions, *Global and Planetary Change*, 108, 158–174,
<https://doi.org/10.1016/j.gloplacha.2013.06.011>, 2013.
- Teruel, O., Rosell-Melè, A., and Penalva-Arias, N.: Global patterns of oceanic dust deposition during Pliocene-Pleistocene
transitions, *EGU21*, <https://doi.org/10.5194/egusphere-egu21-10616>, 2021.
- Thöle, L. M., Amsler, H. E., Moretti, S., Auderset, A., Gilgannon, J., Lippold, J., Vogel, H., Crosta, X., Mazaud, A., Michel,
505 E., Martínez-García, A., and Jaccard, S. L.: Glacial-interglacial dust and export production records from the Southern Indian
Ocean, *Earth and Planetary Science Letters*, 525, 115716, <https://doi.org/10.1016/j.epsl.2019.115716>, 2019.
- Thöle, L. M., Nooteboom, P. D., Hou, S., Wang, R., Nie, S., Michel, E., Sauermilch, I., Marret, F., Sangiorgi, F., and Bijl, P.
K.: An expanded database of Southern Hemisphere surface sediment dinoflagellate cyst assemblages and their oceanographic
affinities, *Journal of Micropalaeontology*, 42, 35–56, <https://doi.org/10.5194/jm-42-35-2023>, 2023.
- 510 Tiedemann, R., Sarnthein, M., and Shackleton, N. J.: Astronomic timescale for the Pliocene Atlantic $\delta^{18}\text{O}$ and dust flux
records of Ocean Drilling Program Site 659, *Paleoceanography*, 9, 619–638, <https://doi.org/10.1029/94PA00208>, 1994.
- Tierney, J. E. and Tingley, M. P.: A Bayesian, spatially-varying calibration model for the TEX₈₆ proxy, *Geochimica et
Cosmochimica Acta*, 127, 83–106, <https://doi.org/10.1016/j.gca.2013.11.026>, 2014.
- Toggweiler, J. R., Russell, J. L., and Carson, S. R.: Midlatitude westerlies, atmospheric CO₂, and climate change during the
515 ice ages: WESTERLIES AND CO₂ DURING THE ICE AGES, *Paleoceanography*, 21, n/a-n/a,
<https://doi.org/10.1029/2005PA001154>, 2006.
- Van der Weijst, C. M. H., van der Laan, K. J., Peterse, F., Reichert, G.-J., Sangiorgi, F., Schouten, S., Veenstra, T. J. T., and
Sluijs, A.: A 15-million-year surface- and subsurface-integrated TEX₈₆ temperature record from the eastern equatorial Atlantic,
Climate of the Past, 18, 1947–1962, <https://doi.org/10.5194/cp-18-1947-2022>, 2022.
- 520 Weiffenbach, J. E., Dijkstra, H. A., von der Heydt, A. S., Abe-Ouchi, A., Chan, W.-L., Chandan, D., Feng, R., Haywood, A.
M., Hunter, S. J., Li, X., Otto-Bliesner, B. L., Peltier, W. R., Stepanek, C., Tan, N., Tindall, J. C., and Zhang, Z.: Highly
stratified mid-Pliocene Southern Ocean in PlioMIP2, *Climate of the Past Discussions*, 1–26, <https://doi.org/10.5194/cp-2023-83>, 2023.
- Westerhold, T., Marwan, N., Drury, A. J., Liebrand, D., Agnini, C., Anagnostou, E., Barnet, J. S. K., Bohaty, S. M., De
525 Vleeschouwer, D., Florindo, F., Frederichs, T., Hodell, D. A., Holbourn, A. E., Kroon, D., Laurentano, V., Littler, K., Lourens,
L. J., Lyle, M., Pälike, H., Röhl, U., Tian, J., Wilkens, R. H., Wilson, P. A., and Zachos, J. C.: An astronomically dated record
of Earth's climate and its predictability over the last 66 million years, *Science*, 369, 1383–1387,
<https://doi.org/10.1126/science.aba6853>, 2020.
- Yamane, M., Yokoyama, Y., Abe-Ouchi, A., Obrochta, S., Saito, F., Moriwaki, K., and Matsuzaki, H.: Exposure age and ice-
530 sheet model constraints on Pliocene East Antarctic ice sheet dynamics, *Nat Commun*, 6, 7016,
<https://doi.org/10.1038/ncomms8016>, 2015.



- Yan, Y., Bender, M. L., Brook, E. J., Clifford, H. M., Kemeny, P. C., Kurbatov, A. V., Mackay, S., Mayewski, P. A., Ng, J., Severinghaus, J. P., and Higgins, J. A.: Two-million-year-old snapshots of atmospheric gases from Antarctic ice, *Nature*, 574, 663–666, <https://doi.org/10.1038/s41586-019-1692-3>, 2019.
- 535 Zhang, Z., Nisancioglu, K. H., and Ninnemann, U. S.: Increased ventilation of Antarctic deep water during the warm mid-Pliocene, *Nat Commun*, 4, 1499, <https://doi.org/10.1038/ncomms2521>, 2013.
- Zhang, Z., Li, X., Guo, C., Otterå, O. H., Nisancioglu, K. H., Tan, N., Contoux, C., Ramstein, G., Feng, R., Otto-Bliesner, B. L., Brady, E., Chandan, D., Peltier, W. R., Baatsen, M. L. J., von der Heydt, A. S., Weiffenbach, J. E., Stepanek, C., Lohmann, G., Zhang, Q., Li, Q., Chandler, M. A., Sohl, L. E., Haywood, A. M., Hunter, S. J., Tindall, J. C., Williams, C., Lunt, D. J.,
- 540 Chan, W.-L., and Abe-Ouchi, A.: Mid-Pliocene Atlantic Meridional Overturning Circulation simulated in PlioMIP2, *Climate of the Past*, 17, 529–543, <https://doi.org/10.5194/cp-17-529-2021>, 2021.
- Ziegler, M., Diz, P., Hall, I. R., and Zahn, R.: Millennial-scale changes in atmospheric CO₂ levels linked to the Southern Ocean carbon isotope gradient and dust flux, *Nature Geosci*, 6, 457–461, <https://doi.org/10.1038/ngeo1782>, 2013.